



Published in final edited form as:

Retina. 2015 July ; 35(7): 1339–1350. doi:10.1097/IAE.0000000000000471.

## Outer Retinal Tubulation in Advanced Age-Related Macular Degeneration: Optical Coherence Tomographic Findings Correspond to Histology

Karen B. Schaal, MD<sup>1</sup>, K. Bailey Freund, MD<sup>1</sup>, Katie M. Litts, BS<sup>2,3</sup>, Yuhua Zhang, PhD<sup>2</sup>, Jeffrey D. Messinger, DC<sup>2</sup>, and Christine A. Curcio, PhD<sup>2</sup>

<sup>1</sup>Vitreous Retina Macula Consultants of New York, New York, USA

<sup>2</sup>Department of Ophthalmology, University of Alabama School of Medicine, Birmingham, Alabama, USA

<sup>3</sup>Vision Science Graduate Program, University of Alabama at Birmingham, Birmingham, Alabama, USA

### Abstract

**Purpose**—To compare optical coherence tomography (OCT) and histology of outer retinal tubulation (ORT) secondary to advanced age-related macular degeneration (AMD) in patients and in post-mortem specimens, with particular attention to the basis of the hyper-reflective border of ORT.

**Method**—A private referral practice (imaging) and an academic research laboratory (histology) collaborated on two retrospective case series. High-resolution OCT raster scans of 43 eyes (34 patients) manifesting ORT secondary to advanced AMD were compared to high-resolution histological sections through the fovea and superior perifovea of donor eyes (13 atrophic AMD and 40 neovascular AMD) preserved 4 hours after death.

**Results**—ORT seen on OCT corresponded to histologic findings of tubular structures comprised largely of cones lacking outer segments (OS) and lacking inner segments (IS). Four phases of cone degeneration were histologically distinguishable in ORT luminal walls, nascent, mature, degenerate, and end-stage (IS and OS; IS only; no IS; no photoreceptors and only Müller cells forming external limiting membrane, ELM, respectively). Mitochondria, which are normally long and bundled within IS ellipsoids, were small and scattered within shrunken IS and cell bodies of surviving cones. A luminal border was delimited by an ELM. ORT observed in closed and open configurations were distinguishable from cysts and photoreceptor islands on both OCT and histology. Hyper-reflective luminal material seen on OCT represents trapped retinal pigment epithelium (RPE) and non-RPE cells.

**Conclusions**—The defining OCT features of ORT are location in the outer nuclear layer (ONL), a hyper-reflective band differentiating it from cysts, and RPE that is either dysmorphic or absent. ORT histologic and OCT findings corresponded in regard to composition, location, shape, and

stages of formation. The reflectivity of ORT luminal walls on OCT apparently does not require an OS or an IS/OS junction, indicating an independent reflectivity source, possibly mitochondria, in the IS.

### Keywords

Photoreceptors; Müller cells; age-related macular degeneration; outer retinal tubulation; ellipsoid; reflectivity; optical coherence tomography; histology; transmission electron microscopy; mitochondria

---

### Introduction

Outer Retinal Tubulation (ORT) was first described histologically as interconnecting tubes containing degenerate photoreceptors and enveloping Müller cells in age-related macular degeneration (AMD).<sup>1</sup> Carbonic-anhydrase histochemistry revealed that ORT is comprised primarily of red-green cones.<sup>1</sup> Processes of Müller cells, normally interleaved between the photoreceptor inner fibers (axons) in the Henle fiber layer,<sup>2-4</sup> in ORT are also reflected externally, wrapping around the surviving cones.<sup>1</sup>

Independently, ORT was designated as a distinctive spectral domain optical coherence tomography (SD-OCT) signature of a thick reflective line surrounding a sometimes extensive and branching hypo-reflective cavity, all within the outer nuclear layer (ONL).<sup>5</sup> A hyper-reflective border distinguishes ORT from cysts, which lack this band, in addition to the relative refractoriness of ORT to anti-vascular endothelial growth factor (VEGF) therapy, compared to cysts. ORT is common in advanced AMD<sup>5-8</sup> and is less common in a variety of other retinal disorders.<sup>5, 9-14</sup> ORT may delimit the border of geographic atrophy (GA) and can be observed overlying fibrotic scars.<sup>7</sup> ORT is typically found in areas of previous outer retinal damage. ORT could be described as a response to “death from below”, i.e. failure of the photoreceptor support system (RPE and choroid) as in choroideremia and some other inherited retinal degenerations.<sup>9, 10</sup> ORT is long lasting,<sup>6</sup> and associated with poor visual outcome in anti-VEGF therapy. Proper recognition of ORT is important clinically, for discriminating its presence from ongoing neovascular activity.<sup>5, 6, 11</sup>

Our goals were to describe histological characteristics of ORT, identify correlates of known clinical imaging features, and informed and motivated by the histological findings, to seek new imaging features. We especially sought a basis for the reflective ORT border, which previous histology suggested could contain the external limiting membrane (ELM), photoreceptor inner segments (IS), or both. Our results demonstrate the sub cellular-level detail available to current generation SD-OCT, and provide evidence for an independent reflectivity source in cone IS in ORT.

### Methods

This study was approved by the Institutional Review Board at UAB (histology) and the Western Institutional Review Board (imaging) and was compliant with the Health Insurance Portability and Accountability Act.

## Histology

We evaluated donor eyes accessioned for research from the Alabama Eye Bank (1995-2012) for the presence of ORT. Median death-to-preservation time was 2:40 hours. Eyes were preserved by immersion in 1% paraformaldehyde and 2.5% glutaraldehyde in 0.1M Sorenson's phosphate buffer (pH 7.2) following anterior segment removal. Donor eyes with gross macular appearance consistent with AMD were processed. Tissue was post-fixed by osmium tannic acid paraphenylenediamine to accentuate extracellular neutral lipids<sup>15, 16</sup> and embedded in epoxy resin (Poly bed 812, Poly sciences, Warrington PA). Macula-wide, 0.8  $\mu\text{m}$ -thick sections<sup>17, 18</sup> at 2 mm superior to the foveal center and through the foveola were stained with toluidine blue. Sections were imaged with a 60 $\times$  oil-immersion objective (numerical aperture = 1.4) and a digital camera (XC10, Olympus). Sections were reviewed in a systematic and unbiased manner.<sup>18</sup> Scanned histological sections are available online at <http://projectmacula>.

Eyes containing apparent, well-preserved mitochondria were selected for further investigation by transmission electron microscopy (TEM), thin-sectioned at silver-gold, and viewed with a 1200 EXII electron microscope (JEOL USA, Peabody, MA) and an AMTXR-40 camera (Advanced Microscopy Techniques, Danvers, MA). Not all ORT identified by light microscopy were imaged, because only one 2 mm region of interest in each 8-mm section fit on a copper grid for TEM. Any ORT in that region was imaged even if not the original ORT of interest. All images were composited with adjustments for exposure, contrast, and background color correction only (Photoshop CS6, Adobe Systems, USA).

## SD-OCT

Thirty-four patients with known advanced AMD and previously identified ORT were selected. All volume scans for each patient were reviewed to find those of the highest quality. OCT raster scans were acquired with a SD-OCT system with image averaging (Spectralis, Heidelberg-Engineering, Heidelberg, Germany). Due to the retrospective nature of this study, scan pattern (i.e., area covered, number of B-scans, and spacing between adjacent B-scans) varied between patients. Spacing ranged from 11  $\mu\text{m}$  to 242  $\mu\text{m}$ , with the densest scanning pattern (11  $\mu\text{m}$ ) showing more detail especially in branching ORT. The presence or absence of a certain ORT finding was recorded, and the best-correlated OCT scan selected. Image quality and therefore image information was variable. Scan quality was reduced mostly due to poor fixation, dry eye, and/or cataract.

Nomenclature for the outer retinal hyper-reflective bands followed Spaide and Curcio<sup>19</sup> and a recently published proposed lexicon,<sup>20</sup> which included the external limiting membrane (ELM) and inner segment ellipsoid (ISel). As recommended, we subdivided the hyporeflective OCT band commonly called ONL into an outer portion, the anatomical ONL and an inner portion, the Henle fiber layer.<sup>21, 22</sup>

## Results

### Histology findings

Forty eyes of 40 donors with neovascular AMD (26 women, 14 men;  $85.5 \pm 7.1$  years) and 13 eyes of 12 donors with geographic atrophy (9 women, 4 men;  $85.7 \pm 4.4$  years), all non-diabetic Caucasian, were reviewed by light microscopy. In 25/40 neovascular AMD eyes (62.5%; 17 women, 4 men;  $86.2 \pm 6.1$  years) and 3/13 geographic atrophy eyes (23.1%; 2 women, 1 man,  $86.3 \pm 9.6$  years), a total of 77 ORT cross-sections were encountered. Of these 77, 65 in sections of good quality and staining were imaged by light microscopy to characterize ORT and generate hypotheses for imaging. From these eyes, 13 neovascular AMD eyes (8 women, 5 men;  $84.8 \pm 5.4$  years) and 1 geographic atrophy eye (1 man, 77 years) were imaged by TEM and 30 ORT were identified.

For reference, outer retina in a normal macula is shown (Figures 1A, 2A). The ELM is an interrupted horizontal line of intensely stained junctional complexes between photoreceptor IS and Müller cell processes. Processes travel centrifugally within the Henle fiber sub layer of the outer plexiform layer (OPL). Müller cell bodies are located in the inner nuclear layer (INL). The ONL has rod and cone nuclei distinguishable by size, chromatin pattern, staining density, and position within the ONL. The IS of cone photoreceptors contain pale staining myoids (ISmy), just external to the ELM. Near the outer segment (OS), IS ellipsoids (ISel) have darkly stained vertical streaks, representing closely packed, thin mitochondria (Figure 2A). OS are recognizable by uniform diameter and staining, with parallel, stacked disks.

Cellular ORT constituents are shown in Figures 1-3 and Table 1. An ELM is present at all times and can be considered an ORT requirement. We will refer to 4 histological phases of photoreceptor degeneration apparent in the luminal walls of ORT. These cells are radially oriented with respect to the lumen, except where noted. The *Nascent* phase exhibits both IS and OS protruding into the lumen, (Figure 1B). The *Mature* phase has IS only (Figure 1D, 1H). The *Degenerate* phase has remnant IS, no IS, or IS that are abuminally retracted away from the ELM (Figure 1E). The *End-stage* phase, resembling a funnel in a desolate macula, has no recognizable photoreceptors, just an ELM made by Müller cells (Figure 1F). Robust Müller cell microvilli at the ELM were seen by TEM (Figure 2B-D). Although cones were the predominant ORT photoreceptor, 4/77 (5.2%) of classified ORT had cell bodies consistent with rods (Figure 1D). In ORT lumens were cells that were nucleated (Figure 1H) and thus presumably capable of gene transcription. RPE-derived cells were recognizable by spindle-shaped black melanosomes and green-staining lipofuscin granules (Figure 1A, G). Non-RPE derived cells were small (Figure 1G) or medium with heterogeneous inclusions typical of macrophages (Figure 2B).

Regarding subcellular constituents, ORT cone IS ellipsoids contain mitochondria, recognizable by staining density and texture and confirmed by TEM as reniform organelles containing cristae (Figure 2C). Mitochondria from ORT cones in the *degenerate* phase were sparse and surrounded by a finely granular cytosol lacking other distinctive features or organelles. Abluminally retracted cone cell bodies (Figure 1C) also contained mitochondria (Figure 2C, Figure 3E), as did spheroid cone cell bodies not bordering on the ELM in single sections (not shown). Cone nuclei were always recognizable.

ORT forms, comparisons with other structures, and formative mechanisms are shown in Figure 3. ORT is differentiable from cysts, which contain predominantly fluid and lack an ELM and radially oriented surrounding cells (Figure 3A). Also unlike cysts, ORT is found in closed and open forms (88.3% and 11.1% of classified ORT, respectively). Closed ORT has circular or oval cross-sections, and an ELM border and photoreceptors completely encircle the lumen (Figure 3A; Figure 1A, C-H; Figure 2B, D). Closed ORT could be lined by as few as 3 cones in degenerate phase ( $< 10 \mu\text{m}$  diameter; data not shown). Open ORT, in contrast, has horizontally elongated cross-sections, curving ELM at the ends, and non-photoreceptor cells on the outer aspect (Figure 3B, E). Asymmetric ORT are open, with photoreceptors on a lateral (Figure 3C) or outer aspect only (not shown). ORT is lemniscate in cross-section at apparent branch points (Figure 3D). ORT of all shapes have in common a curved ELM, whereas photoreceptors surviving in islands over fragmented RPE have a flat ELM (Figure 3F). Figure 3E, G show ORT with multiple phases of cone degeneration in a single cross-section.

### SD-OCT findings

ORT was identified in 43 eyes of 34 patients (14 men, 20 women, mean age  $82 \pm 12$  years) with advanced AMD. Thirty-nine eyes showed neovascular AMD, and 4 eyes had GA. Volumes with closely spaced scans ( $11 \mu\text{m}$ ) aided the interpretation of features suggested by single-section histology, including groups of spheroid cones, branches, and scrolling of the ELM and ISel bands, by permitting connections to features with secure identity. The subdivision between Henle fiber layer and anatomical ONL could be visualized by tilting the entry beam at the pupil, or where these layers were perturbed by pathology in subjacent layers (Figure 4D, 4H, 5J, K).<sup>19, 21, 22</sup>

OCT findings corresponded well with histologic findings with regard to all features examined (Table 1). Of special interest were ORT definition, differentiation between open and closed ORT, ORT shape, distinction between ORT and cysts, and distinction between ORT and photoreceptor islands (Figure 4). Closed ORT was found in all patients examined (34 patients, 100%), whereas open ORT was found in 14 patients (41%; uncertain in 5 patients, 15%). Asymmetric ORT, hyper-reflective ‘clouds’ at a variable distance from ORT, different intra-luminal content of ORT, and ORT formation were also correlated (Figure 5). The four phases of cone degeneration identified in histology, although hinted at in some OCT scans, could not be reliably identified (Table 1).

Thirty-one patients (91%) had ORT with hyper-reflective luminal content (unclear in 3 patients, 9%). This hyper-reflective material was large, circular, and free-floating (4 patients, 13%) or small, dappled, and attached to the hyper-reflective border of the ORT (3 patients, 10%) or both (17 patients, 55%). In 7 patients (22%), scan quality did not allow a determination whether intra-luminal material was attached or free-floating.

Branching ORT (Figure 5L, M) was obvious in 20 patients (59%; uncertain in 5 patients, 15%). Asymmetric ORT was found in 9 patients (26%; uncertain in 4 patients, 12%). An area of hyper-reflectivity next to an ORT was seen in 12 patients (35%; uncertain in 5 patients, 15%). Photoreceptor islands were seen in 22 patients (65%; uncertain in 2 patients, 6%). ORT formation via scrolling from an intact photoreceptor layer (forme fruste ORT)

was present in 23 patients (68%; uncertain in one patient). The smallest ORT cross-section identifiable in volume scans was 31  $\mu\text{m}$  in diameter.

The reflective ORT border was examined for continuity with normal ISel and ELM bands surrounding the atrophic area. In Figure 5I, the ELM is wider and more reflective, and the ISel less reflective, at the scroll. We observed reflective material, sometimes continuous like an additional band, internal to and distinct from the ORT border (Figure 4D, 5C, 5J and 5K). This finding could indicate preserved anatomical ISel.

## Discussion

This is the largest number of advanced AMD eyes examined by histology to date specifically for photoreceptor degeneration. A remarkable number of histological features were found to correspond with OCT features (Table 1). It was possible to identify the ELM and IS mitochondria as potential candidates for the reflective border of ORT. Although different eyes were examined clinically and histologically, and only morphologic parameters were assessed, the large sample size and numerous correspondences between the two techniques lend credence to our conclusions. One major insight is that although degenerating cones lose OS early like degenerating rods, ORT cones, which can survive for extended periods,<sup>6</sup> do so largely without OS.

We defined a system of four cone degeneration phases, which in turn directed OCT exploration and identification off our major features of ORT. First, ORT is always located in the ONL, involving both the anatomical ONL and Henle fiber layer, which are not always distinguishable on OCT.<sup>23</sup> Second, on OCT, ORT is defined by a hyper-reflective band in closed or open configuration; on histology, ORT is defined by a circular or ovoid ELM border including IS in *degenerate*, *mature*, and *nascent* phases and IS and OS in the *nascent* phase. Third, the underlying RPE is dysmorphic or absent. Fourth, a 'free edge' to scroll appears to be necessary. We do not consider branching a defining feature because although it is common, not all ORT branch. Groups of spheroid cone cell bodies corresponded to hyper-reflective clouds, which were actually glancing sections of ORT that were more apparent on adjacent scans. We found ORT where the ELM seemed to scroll and encircle the photoreceptors (Figure 5I-K). OCT volume scans revealed a scrolling of the photoreceptor layer that was harder to appreciate by histology due to limited number of sections. Histology suggests that ORT involutes over time, and with the IS shrinking and mitochondria migrating through the ELM towards the cone perikaryon. It is important to note that a staging system for cone degeneration is not a staging system for ORT, but rather a necessary first step. An ORT staging system would ideally include measures of how much of each degeneration phase was present, the overall extent of ORT-affected retina, the duration of ORT existence, distances from less affected retina outside the atrophic area, and branching complexity, since complexity likely declines as ORT involute.

Of the ORT-participating cells, Müller cells appear to be prime movers in formation, apparently sealing off photoreceptors from the RPE-Bruch's complex and remaining in *end-stage* ORT. These findings in AMD parallel long-term experimental retinal detachment.<sup>1, 24</sup> Prominence of the persisting ELM (Figure 1F) may be due to selective survival of

cytoskeleton-rich plaques on the Müller cell side of ELM adherens junctions as cones die.<sup>25, 26</sup> We hypothesize that a requirement for cones and Müller cells with very long processes, found only in the macula, underlies the predilection of ORT for this region. Of interest was the presence of RPE and other cells within the ORT lumen, perhaps providing trophic support to photoreceptors via a connection to less affected retina outside the atrophic area. These cells presumably gain access to the ORT cavity during the scrolling process.

ORT of AMD can be distinguished from rosettes described in other diseases involving photoreceptors by their tubular structure, large size, and degenerative instead of developmental nature. In tumors affecting young children, rosettes are classified into three types based on the degree of retinal differentiation.<sup>27</sup> Homer Wright (HW) rosettes, common in neuroblastoma, contain primitive neuroblastic cells encircling a solid 30-50 µm-diameter central tangle of neural filaments, rather than a lumen.<sup>27</sup> Flexner-Wintersteiner (FW) rosettes, common in retinoblastoma, contain early differentiated photoreceptors surrounding a central lumen 40-60 µm in diameter. Fleurettes are advanced differentiated photoreceptors with IS pointing centrally and lacking a lumen. FW rosettes contain photoreceptors with zonula adherens contacts resembling the ELM, and these cells contain mitochondrial aggregates in IS-like compartments.<sup>28</sup> HW rosettes are arranged in clusters with exclusively circular cross-sections suggesting multiple spheroidal cavities. ORT is distinguishable from several geometrically diverse malformations, also called rosettes, resulting from ONL dysmorphogenesis in mouse inherited retinopathies. These include folds with or without internal cells, inward ONL protrusions, and double layers.<sup>29, 30</sup> Such malformations are attributed to mislocalization and delayed maturation of photoreceptors and can be associated with defective proteins impacting ELM integrity.<sup>30</sup> Patients with retinitis pigmentosa have rosettes<sup>32</sup> and rarely, ORT.<sup>10, 33</sup> A histological description of one rosette in such a patient resembles ORT structurally and contains immunohistochemically confirmed rods.<sup>34</sup>

In this first extensive ultra structural examination of photoreceptor death in human AMD macula, we saw a striking change in cone IS mitochondria from long, thin, and bundled to small, ovoid, and dispersed in ORT. Mitochondria are increasingly seen as central to neurodegeneration,<sup>35-43</sup> as well as being essential for oxidative phosphorylation, intermediary metabolism, redox signaling, calcium buffering, and apoptosis regulation. Tightly bundled IS mitochondria efficiently utilize high oxygen from choroid for phototransduction and contribute to IS optical properties.<sup>19, 44</sup> Mitochondrial morphology is dynamically controlled to respond to energy needs and environmental stimuli by the processes of fusion and fission to form larger and smaller organelles, respectively. Fusion mixes mitochondrial contents and dilutes minimally damaged components among normal organelles. Fission sequesters irreparably damaged components for elimination by mitophagy, a bulk disposal process involving transport towards the soma. Abnormal fusion and fission dynamics contribute to cell death in age-related neurodegenerations like Parkinson and Alzheimer disease. Images of apparent mitochondrial fission and retraction towards cell bodies in ORT hint at similar processes in human cone photoreceptors degenerating secondarily to support system failure in AMD.

Our observations on ORT add important new information to the debate on the histologic correlate of the second outer retinal hyper-reflective band observed with SD-OCT,

commonly called the IS/OS junction. This name assumes a refractive index boundary at the interface and/or change of the wave-guiding properties between the IS and OS of both cone and rods.<sup>45</sup> More recently this band has been ascribed to the ISel based on an anatomically correct outer retinal model<sup>19, 44, 46, 47</sup> and corroborated experimentally.<sup>48</sup> As visualized by adaptive optics-OCT, the perifoveal ISel band is  $\sim 6.0 \mu\text{m}$  thick, too thick for a single reflective plane, and suggestive of the tapered outer half of the anatomical ISel.<sup>49, 50</sup> Comparing OCT scans with histology to test the relative contributions of wave guiding and scattering to band reflectivity has been hindered by the lack of human tissue specimens with perturbed photoreceptor layers, which we herein provide.

The optical complexity of ORT is illustrated by the scroll in Figure 5K (also Figures 4D, 5C, 5I). The hyper-reflective signal closest to the ORT lumen appears stronger when oriented parallel to the RPE. The hyper-reflective signal furthest from the lumen, which appears continuous with the ELM, is stronger and wider when oriented orthogonal to the RPE. The poorer transverse ( $14 \mu\text{m}$ ) vs axial ( $7 \mu\text{m}$ ) resolution of SD-OCT likely contributes to this difference. While raising many new questions, our current data can support four new concepts about reflectivity sources in OCT. First, ORT cones are radially oriented relative to the ORT lumen and variably oriented relative to the direction of light, making the role of wave guiding in producing the ORT reflective border uncertain. Second, photoreceptors in phases beyond nascent lack OS, and thus by definition, lack an IS/OS junction, indicating that the reflective border requires neither OS nor a junction. However, light scatters back from optical interfaces formed by discontinuities of refractive index, and when OS atrophy, new interfaces form between residual IS and their surroundings. Third, IS have independent reflectivity sources. Because mitochondria occupy  $\sim 75\%$  of normal ISel volume,<sup>19</sup> they are obvious candidate scatterers. Mitochondria-associated refractive index gradients may be modulated by metabolic status, organelle shape, and packing within parallel bundles.<sup>44, 49, 51, 52</sup> In ORT, mitochondria alone among organelles persist in atrophied IS, apparently generating a signal even if shrunken, clustered, dispersed, or randomly oriented. Finally, both the ELM and IS mitochondria contribute, although unequally, to the hyper-reflective ORT border. Increased hyper-reflectivity of the foveal ELM in the absence of hyper-reflective cone OS occurs early in patients with achromatopsia, a progressive cone degeneration.<sup>53</sup> Due to mitochondrial translocation towards the nucleus in ORT, both structures co-localize within the light path. However, the ELM is normally so small that it must be logarithmically scaled for visibility in SD-OCT B-scans, so the mitochondrial contribution likely dominates.

Whether our hypotheses about ORT reflectivity sources are applicable to normal photoreceptors remains to be determined. A direct continuity of the reflective border of nascent scrolling ORT with the ISel in unaffected retina surrounding atrophy would be definitive, yet such a transition was difficult to discern. It is possible that tilting the OCT light beam within the entrance pupil via directional OCT would reveal photoreceptors that are present but mis-oriented and thus are poorer waveguides at that critical boundary.<sup>21, 22, 50</sup> Despite these uncertainties, ISel reflectivity has been utilized as a measure of mitochondrial health by investigators motivated by the notion that the ARMS2 gene, a variant of which strongly associates with AMD risk, may encode for a mitochondrial protein<sup>54</sup>. Reduced reflectivity in patients with early AMD was reported.<sup>55, 56</sup> The ISel



attracts interest, due to its correlation with visual acuity and prognostic value in retinal diseases.<sup>57</sup> Defining its correct anatomical substrate thus remains a research priority.

This study had limitations. Different eyes were examined by OCT and histology. The histological encounter rate is not generalizable to the overall prevalence rate of ORT, because these donor eyes were highly selected, and they were accessioned largely before the anti-VEGF era. The much lower proportion of open ORT in histology relative to OCT may reflect classification uncertainty, advanced state of AMD in these eyes relative to those with active neovascular AMD seen clinically, or both. Histological analysis used single sections only. ORT cross-sections are taller on OCT than in histology due to vertical tissue shrinkage during histologic processing and OCT scans vertically stretched for clearer visualization. More ultrastructure from cones at stages between unaffected and entubulated would be useful for testing the mitochondrial reflectivity hypothesis. Additional data from directional OCT and adaptive optics-facilitated retinal imaging could help determine whether cone degeneration phases are visible *in vivo*. An ORT staging system could be generated in longitudinal studies involving closely spaced SD-OCT volume scans.

In conclusion, ORT demonstrates that photoreceptors have an extended will to live even in advanced AMD. Our data will inform the study of macular cone life and death, mitochondrial dynamics, and concomitant Müller cell activity, in clinic populations where high-resolution longitudinal imaging of individual patients is possible. This capability is important, because current animal models of cone degeneration focus on primary neurodegenerations in species lacking long Henle fibers<sup>58, 59</sup>. The complementary approaches of histology and clinical OCT can provide important insight into retinal cell biology, tissue optics, and neurodegeneration.

## Acknowledgments

This work was supported by NIH grants EY06109 (CAC and JDM), 5R21EY021903 (YZ), International Retina Research Foundation (YZ), Eye Sight Foundation of Alabama (YZ), unrestricted funds to the Department of Ophthalmology from Research to Prevent Blindness, Inc. (CAC and YZ), the Vision Science Graduate Program at UAB (KML), and the Macula Foundation (KBF). Acquisition of donor eyes received additional support from International Retinal Research Foundation, National Eye Institute P30 EY003039, and the Arnold and Mabel Beckman Initiative for Macular Research. Creation of Project MACULA received additional support from the Edward N. and Della L. Thome Memorial Foundation. We thank the Alabama Eye Bank for timely retrieval of donor eyes.

## References

1. Curcio CA, Medeiros NE, Millican CL. Photoreceptor loss in age-related macular degeneration. *Invest Ophthalmol Vis Sci.* 1996; 37:1236–49. [PubMed: 8641827]
2. Tsukamoto Y, Masarachia P, Schein SJ, Sterling P. Gap junctions between the pedicles of macaque foveal cones. *Vision Res.* 1992; 32:1809–15. [PubMed: 1337638]
3. Drasdo N, Millican CL, Katholi CR, Curcio CA. The length of Henle fibers in the human retina and a model of ganglion receptive field density in the visual field. *Vision Res.* 2007; 47:2901–11. [PubMed: 17320143]
4. Polyak, SL. *The Vertebrate Visual System.* Chicago: University of Chicago; 1957.
5. Zweifel SA, Engelbert M, Laud K, et al. Outer retinal tubulation: a novel optical coherence tomography finding. *Arch Ophthalmol.* 2009; 127:1596–602. [PubMed: 20008714]

6. Jung JJ, Freund KB. Long-term Follow-up of Outer Retinal Tubulation Documented by Eye-Tracked and En Face Spectral-Domain Optical Coherence Tomography. *Arch Ophthalmol.* 2012; 130:1618–9. [PubMed: 23229712]
7. Wolff B, Matet A, Vasseur V, et al. En Face OCT Imaging for the Diagnosis of Outer Retinal Tubulations in Age-Related Macular Degeneration. *J Ophthalmol.* 2012; 2012:542417. [PubMed: 22970349]
8. Moussa K, Lee JY, Stinnett SS, Jaffe GJ. Spectral domain optical coherence tomography-determined morphologic predictors of age-related macular degeneration-associated geographic atrophy progression. *Retina.* 2013; 33:1590–9. [PubMed: 23538573]
9. Goldberg NR, Greenberg JP, Laud K, et al. Outer Retinal Tubulation in Degenerative Retinal Disorders Retina. 2013
10. Iriyama A, Aihara Y, Yanagi Y. Outer retinal tubulation in inherited retinal degenerative disease. *Retina.* 2013; 33:1462–5. [PubMed: 23538577]
11. Papastefanou VP, Nogueira V, Hay G, et al. Choroidal naevi complicated by choroidal neovascular membrane and outer retinal tubulation. *Br J Ophthalmol.* 2013; 97:1014–9. [PubMed: 23686326]
12. Fujinami K, Sergouniotis PI, Davidson AE, et al. Clinical and molecular analysis of Stargardt disease with preserved foveal structure and function. *Am J Ophthalmol.* 2013; 156:487–501 e1. [PubMed: 23953153]
13. Sergouniotis PI, Davidson AE, Lenassi E, et al. Retinal structure, function, and molecular pathologic features in gyrate atrophy. *Ophthalmology.* 2012; 119:596–605. [PubMed: 22182799]
14. Ellabban AA, Hangai M, Yamashiro K, et al. Tomographic fundus features in pseudoxanthoma elasticum: comparison with neovascular age-related macular degeneration in Japanese patients. *Eye (Lond).* 2012; 26:1086–94. [PubMed: 22653517]
15. Guyton JR, Klemp KF. Ultra structural discrimination of lipid droplets and vesicles in atherosclerosis: value of osmium-thiocarbohydrazide-osmium and tannic acid-paraphenylenediamine techniques. *J Histochem Cytochem.* 1988; 36:1319–28. [PubMed: 2458408]
16. Curcio CA, Millican CL, Bailey T, Kruth HS. Accumulation of cholesterol with age in human Bruch's membrane. *Invest Ophthalmol Vis Sci.* 2001; 42:265–74. [PubMed: 11133878]
17. Curcio CA, Messinger JD, Sloan KR, et al. Human chorioretinal layer thicknesses measured in macula-wide, high-resolution histologic sections. *Invest Ophthalmol Vis Sci.* 2011; 52:3943–54. [PubMed: 21421869]
18. Curcio CA, Messinger JD, Sloan KR, et al. Subretinal drusenoid deposits in non-neovascular age-related macular degeneration: morphology, prevalence, topography, and biogenesis model. *Retina.* 2013; 33:265–76. [PubMed: 23266879]
19. Spaide RF, Curcio CA. Anatomical correlates to the bands seen in the outer retina by optical coherence tomography: literature review and model. *Retina.* 2011; 31:1609–19. [PubMed: 21844839]
20. Staurenghi G, Sadda S, Chakravarthy U, et al. Proposed Lexicon for Anatomic Landmarks in Normal Posterior Segment Spectral-Domain Optical Coherence Tomography: The IN\*OCT Consensus. *Ophthalmology.* 2014
21. Lujan BJ, Roorda A, Knighton RW, Carroll J. Revealing Henle's fiber layer using spectral domain optical coherence tomography. *Invest Ophthalmol Vis Sci.* 2011; 52:1486–92. [PubMed: 21071737]
22. Mrejen S, Gallego-Pinazo R, Freund KB, Paques M. Recognition of Henle's fiber layer on OCT images. *Ophthalmology.* 2013; 120:e32–3 e1. [PubMed: 23732066]
23. Otani T, Yamaguchi Y, Kishi S. Improved visualization of Henle fiber layer by changing the measurement beam angle on optical coherence tomography. *Retina.* 2011; 31:497–501. [PubMed: 21102368]
24. Anderson DH, Guerin CJ, Erickson PA, et al. Morphological recovery in the reattached retina. *Invest Ophthalmol Vis Sci.* 1986; 27:168–83. [PubMed: 3943943]
25. Williams DS, Arikawa K, Paallysaho T. Cytoskeletal components of the adherens junctions between the photoreceptors and the supportive Muller cells. *J Comp Neurol.* 1990; 295:155–64. [PubMed: 2341633]

26. Omri S, Omri B, Savoldelli M, et al. The outer limiting membrane (OLM) revisited: clinical implications. *Clin Ophthalmol.* 2010; 4:183–95. [PubMed: 20463783]
27. Eagle RC Jr. The pathology of ocular cancer. *Eye (Lond).* 2013; 27:128–36. [PubMed: 23154492]
28. Ts'o MO, Fine BS, Zimmerman LE. The Flexner-Wintersteiner rosettes in retinoblastoma. *Arch Pathol.* 1969; 88:664–71. [PubMed: 5357720]
29. Fischer MD, Huber G, Beck SC, et al. Noninvasive, in vivo assessment of mouse retinal structure using optical coherence tomography. *PLoS One.* 2009; 4:e7507. [PubMed: 19838301]
30. Stuck MW, Conley SM, Naash MI. Defects in the outer limiting membrane are associated with rosette development in the Nrl<sup>-/-</sup> retina. *PLoS One.* 2012; 7:e32484. [PubMed: 22427845]
31. van de Pavert SA, Kantardzhieva A, Malysheva A, et al. Crumbs homologue 1 is required for maintenance of photoreceptor cell polarization and adhesion during light exposure. *J Cell Sci.* 2004; 117:4169–77. [PubMed: 15316081]
32. Milam AH, Jacobson SG. Photoreceptor rosettes with blue cone opsin immune reactivity in retinitis pigmentosa. *Ophthalmology.* 1990; 97:1620–1631. [PubMed: 2150875]
33. Goldberg NR, Greenberg JP, Laud K, et al. Outer retinal tubulation in degenerative retinal disorders. *Retina.* 2013; 33:1871–6. [PubMed: 23676993]
34. Tulvatana W, Adamian M, Berson EL, Dryja TP. Photoreceptor rosettes in autosomal dominant retinitis pigmentosa with reduced penetrance. *Arch Ophthalmol.* 1999; 117:399–402. [PubMed: 10088824]
35. McInnes J. Insights on altered mitochondrial function and dynamics in the pathogenesis of neurodegeneration. *Transl Neurodegener.* 2013; 2:12. [PubMed: 23711354]
36. Maresca A, la Morgia C, Caporali L, et al. The optic nerve: a “mito-window” on mitochondrial neurodegeneration. *Mol Cell Neuro sci.* 2013; 55:62–76.
37. Youle RJ, vander Blik AM. Mitochondrial fission, fusion, and stress. *Science.* 2012; 337:1062–5. [PubMed: 22936770]
38. Federico A, Cardaioli E, Da Pozzo P, et al. Mitochondria, oxidative stress and neurodegeneration. *J Neurol Sci.* 2012; 322:254–62. [PubMed: 22669122]
39. Chen H, Chan DC. Critical dependence of neurons on mitochondrial dynamics. *Curr Opin Cell Biol.* 2006; 18:453–9. [PubMed: 16781135]
40. Chen H, Chan DC. Mitochondrial dynamics--fusion, fission, movement, and mitophagy--in neurodegenerative diseases. *Hum Mol Genet.* 2009; 18:R169–76. [PubMed: 19808793]
41. Knott AB, Perkins G, Schwarzenbacher R, Bossy-Wetzl E. Mitochondrial fragmentation in neurodegeneration. *Nat Rev Neuro sci.* 2008; 9:505–18.
42. Bossy-Wetzl E, Barsoum MJ, Godzik A, et al. Mitochondrial fission in apoptosis, neurodegeneration and aging. *Curr Opin Cell Biol.* 2003; 15:706–16. [PubMed: 14644195]
43. MacAskill AF, Kittler JT. Control of mitochondrial transport and localization in neurons. *Trends Cell Biol.* 2010; 20:102–12. [PubMed: 20006503]
44. Hoang QV, Linsenmeier RA, Chung CK, Curcio CA. Photoreceptor inner segments in monkey and human retina: mitochondrial density, optics, and regional variation. *Vis Neurosci.* 2002; 19:395–407. [PubMed: 12511073]
45. Hood DC, Zhang X, Ramachandran R, et al. The inner segment/outer segment border seen on optical coherence tomography is less intense in patients with diminished cone function. *Invest Ophthalmol Vis Sci.* 2011; 52:9703–9. [PubMed: 22110066]
46. Fernandez EJ, Hermann B, Povazay B, et al. Ultra high resolution optical coherence tomography and pan correction for cellular imaging of the living human retina. *Opt Express.* 2008; 16:11083–94. [PubMed: 18648422]
47. Huang Y, Cideciyan AV, Papastergiou GI, et al. Relation of optical coherence tomography to microanatomy in normal and rd chickens. *Invest Ophthalmol Vis Sci.* 1998; 39:2405–16. [PubMed: 9804149]
48. Lu RW, Curcio CA, Zhang Y, et al. Investigation of the hyper-reflective inner/outer segment band in optical coherence tomography of living frog retina. *J Biomed Opt.* 2012; 17:060504. [PubMed: 22734727]

49. Meadway A, Girkin CA, Zhang Y. A dual-modal retinal imaging system with adaptive optics. *Opt Express*. 2013; 21:29792–807. [PubMed: 24514529]
50. Panorgias A, Zawadzki RJ, Capps AG, et al. Multimodal assessment of microscopic morphology and retinal function in patients with geographic atrophy. *Invest Ophthalmol Vis Sci*. 2013; 54:4372–84. [PubMed: 23696601]
51. Wilson JD, Cottrell WJ, Foster TH. Index-of-refraction-dependent subcellular light scattering observed with organelle-specific dyes. *J Biomed Opt*. 2007; 12:014010. [PubMed: 17343485]
52. Tychinsky V. The metabolic component of cellular refractivity and its importance for optical cytometry. *J Biophotonics*. 2009; 2:494–504. [PubMed: 19644930]
53. Greenberg JP, Sherman J, Zweifel SA, et al. Spectral-domain optical coherence tomography staging and auto fluorescence imaging in achromatopsia. *JAMA Ophthalmol*. 2014; 132:437–45. [PubMed: 24504161]
54. Fritsche LG, Loenhardt T, Janssen A, et al. Age-related macular degeneration is associated with an unstable ARMS2 (LOC387715) mRNA. *Nat Genet*. 2008; 40:892–6. [PubMed: 18511946]
55. Wu Z, Ayton LN, Guymer RH, Luu CD. Second reflective band intensity in age-related macular degeneration. *Ophthalmology*. 2013; 120:1307–8 e1. [PubMed: 23732057]
56. Wu Z, Ayton LN, Guymer RH, Luu CD. Relationship between the second reflective band on optical coherence tomography and multifocal electroretinography in age-related macular degeneration. *Invest Ophthalmol Vis Sci*. 2013; 54:2800–6. [PubMed: 23532524]
57. Wong IY, Iu LP, Koizumi H, Lai WW. The inner segment/outer segment junction: what have we learnt so far? *Curr Opin Ophthalmol*. 2012; 23:210–8. [PubMed: 22450219]
58. Xu J, Morris L, Thapa A, et al. cGMP accumulation causes photoreceptor degeneration in CNG channel deficiency: evidence of cGMP cyto toxicity independently of enhanced CNG channel function. *J Neurosci*. 2013; 33:14939–48. [PubMed: 24027293]
59. Ding XQ, Harry CS, Umino Y, et al. Impaired cone function and cone degeneration resulting from CNGB3 deficiency: down-regulation of CNGA3 biosynthesis as a potential mechanism. *Hum Mol Genet*. 2009; 18:4770–80. [PubMed: 19767295]

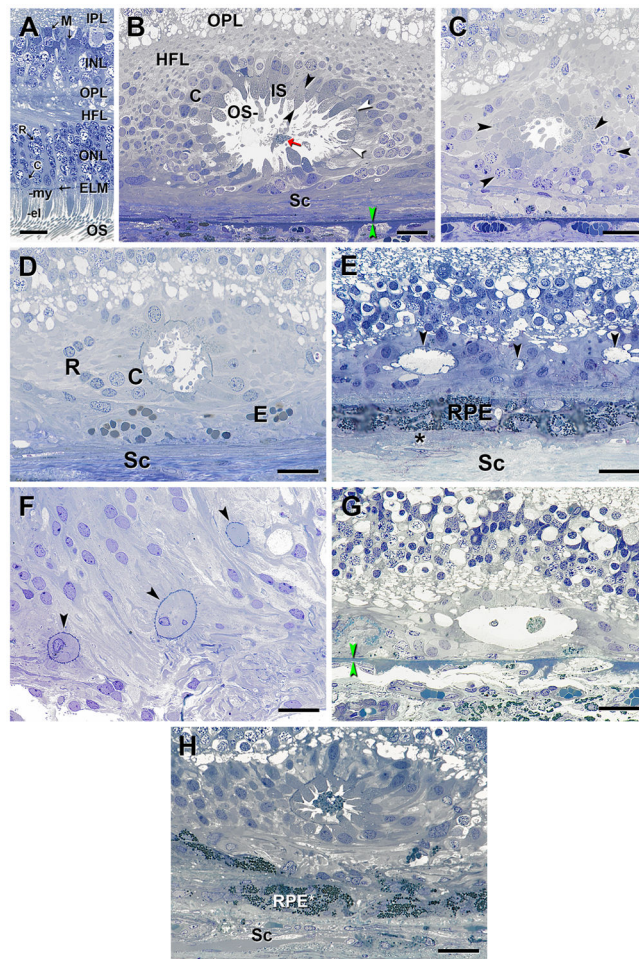


### Figure 1. Cellular constituents of ORT in neovascular AMD

Toluidine blue stained, 0.8  $\mu\text{m}$  thick sections of maculas post-fixed by osmium-tannic acid-paraformaldehyde method. INL, inner nuclear layer; OPL syn, outer plexiform layer, pedicles and spherules; HFL, Henle fiber layer (containing photoreceptor and Müller cell fibers); ONL, outer nuclear layer (R=rods, C=cones); ELM, external limiting membrane; IS, photoreceptor inner segments; my, myoid; el, ellipsoid; OS, outer segments. Bars = 25  $\mu\text{m}$ .

**A.** Photoreceptors at 2.5 mm temporal to the foveal center in a healthy macula. Rod and cone nuclei are distinguishable by size, chromatin patterns, staining, and position relative to ELM. ISmy (-my) is pale. ISel (-el) has darkly stained vertical streaks indicating closely packed, thin mitochondria. M, Müller cell nuclei in the INL. Due to artifactual post-mortem detachment, OS are bent, en masse, in parallel. 85 yr old woman. **B.** Closed ORT. Cone nuclei (C) surround a lumen delimited by the ELM (white arrowheads). Cone IS, some with OS, protrude into the lumen, maintaining a radial organization with respect to the lumen center. IS have mitochondria-containing ellipsoids and less frequently, myoids (one cell containing both indicated by black arrowheads). One cell with green-staining lipofuscin granules is in the lumen (red arrow). HFL contains darkly stained cone fibers in cross-section. Sc, fibrocellular scar. Green arrowheads, Bruch's membrane, which is breached in this panel. 79 yr old man. **C.** Cone cell bodies (arrowheads), spheroid in shape, are retracted

from the lumen yet contain mitochondria. 83 yr old man. **D.** Apparent rod cell bodies (flanking R) as well as cones (flanking C) in a closed ORT. E, erythrocytes; Sc, fibrocellular scar secondary to CNV. 79 yr old man. **E.** Three ORT recognizable by ELM border only (arrows) and lacking IS protruding into the lumen; RPE, retinal pigment epithelium; \*, persistent basal laminar deposit overlying neo-capillaries; Sc, fibrocellular scar subsequent to type I CNV; 82 yr old woman. **F.** Three end-stage ORT (arrowheads). Cells contributing to ELM are all Müller cells, as no photoreceptors survived in this desolate macula. 90 yr old woman. **G.** Cells in ORT lumen are RPE-derived with green-staining lipofuscin granules (right) and non-RPE derived (left) overlying ghost choriocapillaries. Arrowheads, Bruch's membrane; 80 yr old woman. **H.** Nucleated RPE cell within an ORT lumen; RPE\*, RPE-derived cells with spherical melanosomes; Sc, fibrovascular scar; 87 yr old man.

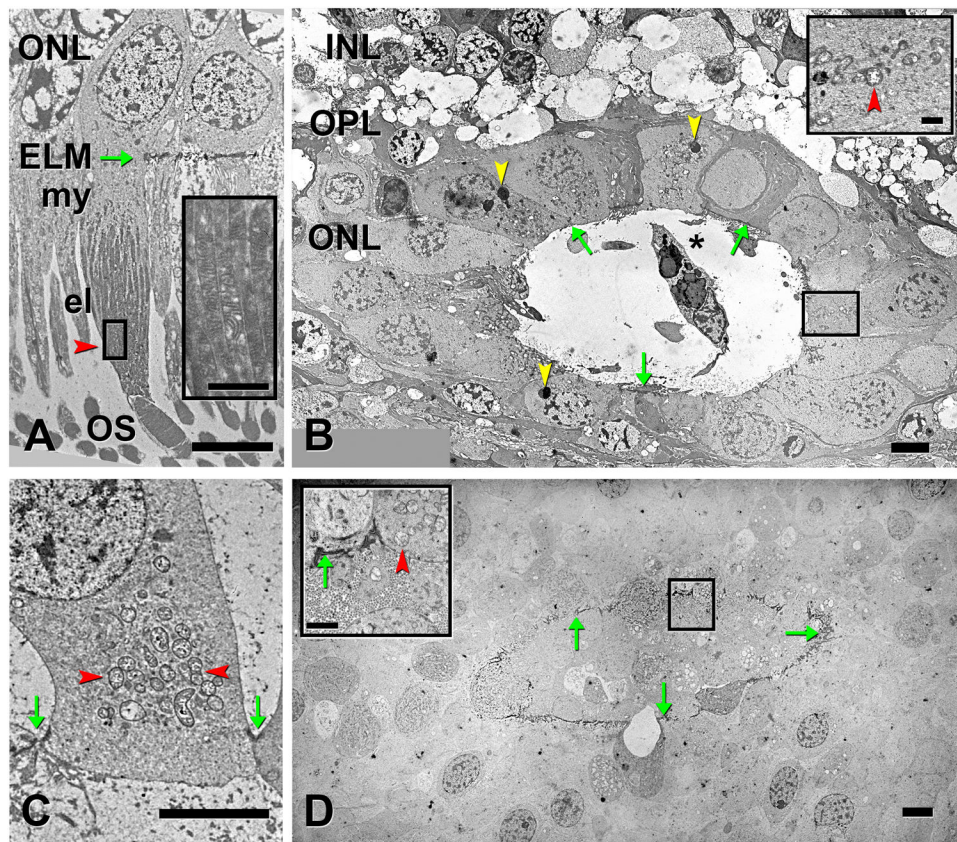


**Figure 2. Sub cellular constituents of ORT visible by transmission electron microscopy**  
 Green arrows point to ELM, and red arrowhead point to mitochondria, in all panels. **A.** Photoreceptors at 2.5 mm temporal to the foveal center in a healthy macula. Electron dense mitochondria (red arrowheads) are thin and tightly packed in the ISel (Inset, magnified box.) 85 yr old woman. **B.** Degenerate ORT containing macrophage (asterisk) in lumen at 3.2 mm temporal to the foveal center. Mitochondria translocated from ISel to area between ELM (green arrows) and cone nucleus. Cone lipofuscin (yellow arrowheads) are electron dense granules. Inset, mitochondria in the same photoreceptor on an adjacent section. 85 yr old woman. **C.** Cone in ORT showing mitochondria clustered between ELM and nucleus (between red arrowheads); located 3.2 mm from foveal center. **D.** ORT denoted by continuous ELM containing Müller cell and photoreceptor cross sections; located at 2.4 mm nasal to foveal center. Inset, magnified box of ELM, Müller cell microvilli in cross-section, and mitochondria. 79 yr old man. Inset scale bars 1  $\mu\text{m}$ . Other scale bars 5  $\mu\text{m}$ .

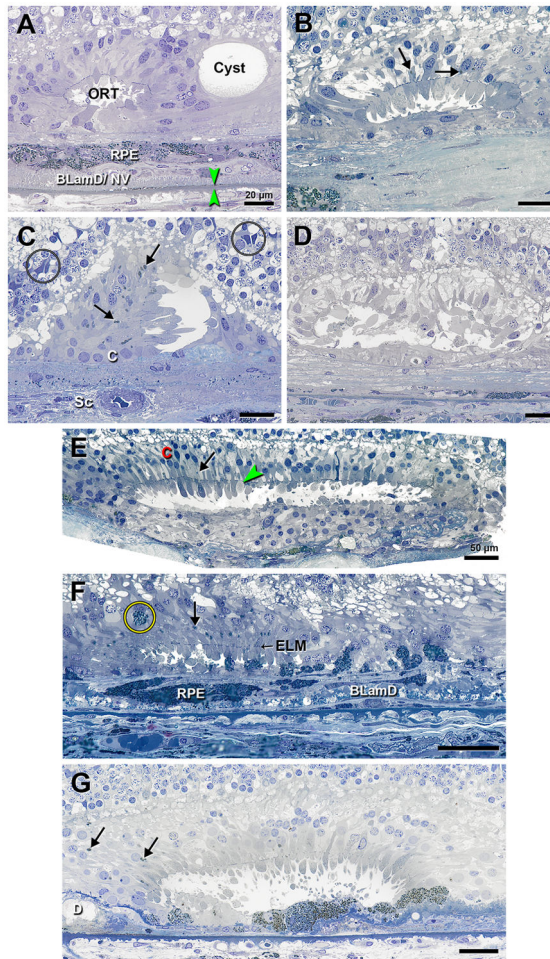


### Figure 3. ORT forms, differentials, and biogenesis by histology

Neovascular AMD, except where noted. Histological preparation details and labeling conventions are described in Figure 1 caption. Bars A-D, 20  $\mu$ m; bars E-G, 50  $\mu$ m. **A.** Closed ORT have circular or oval cross-sections, with an ELM border and photoreceptors that completely encircle the lumen. ORT are distinguishable from cysts, which lack an ELM and an organized arrangement of surrounding cells and contains predominantly fluid. RPE is multilayered and overlies persistent rivulet basal laminar deposits with neovascularization (BLamD/NV). Basal linear deposit is apparent on the surface of Bruch's membrane (arrowheads) 87 yr old woman. **B.** Open ORT has horizontally elongated cross-sections, curving ELM at the ends, and an absence of photoreceptors on the outer aspect; arrow, cone lipofuscin; 77 yr old woman. **C.** Asymmetric ORT has photoreceptors on a lateral or outer aspect of the lumen only; C, cone nuclei. Müller cell nuclei in INL are circled. Arrows, cone lipofuscin. Sc, fibrovascular scar; 79 yr old man. **D.** Open ORT with a lemniscate cross-sectional profile attributed to a branch point. ORT has various cells in lumen and Müller cells with watery cytoplasm. **E.** Flat, closed ORT with cone nuclei (C) and ISeI mitochondria, which have retracted inwardly from the ELM (green arrowhead) and from the IS. Spheroid cones have piled up on the outer aspect. Arrow, cone lipofuscin; 87 yr old woman **F.** Surviving island of photoreceptors, not considered an ORT because the ELM



(small arrow) is not curved at the ends. Yellow circle, intra-retinal RPE; large arrow, cone lipofuscin; RPE, hyper-pigmented RPE-derived cells within sub-retinal fibrocellular scar; B Lam D, persistent basal laminar deposit overlying neovascular membrane; 94 yr old woman. **G.** An open ORT exhibits different stages of maturity along the luminal wall, suggesting ORT dynamism. On the right are nearly continuous RPE, IS with myoid and ellipsoids, moderately retracted cone nuclei, and remnant OS. On the left are RPE fragments, IS only with mitochondria retracted behind the ELM, and cone nuclei retracted to a more inward level relative to the right. Persistent basal laminar deposits and neuroglial scar underlie RPE throughout. D, calcified druse. Arrow, cone lipofuscin. 87 yr old man with geographic atrophy.

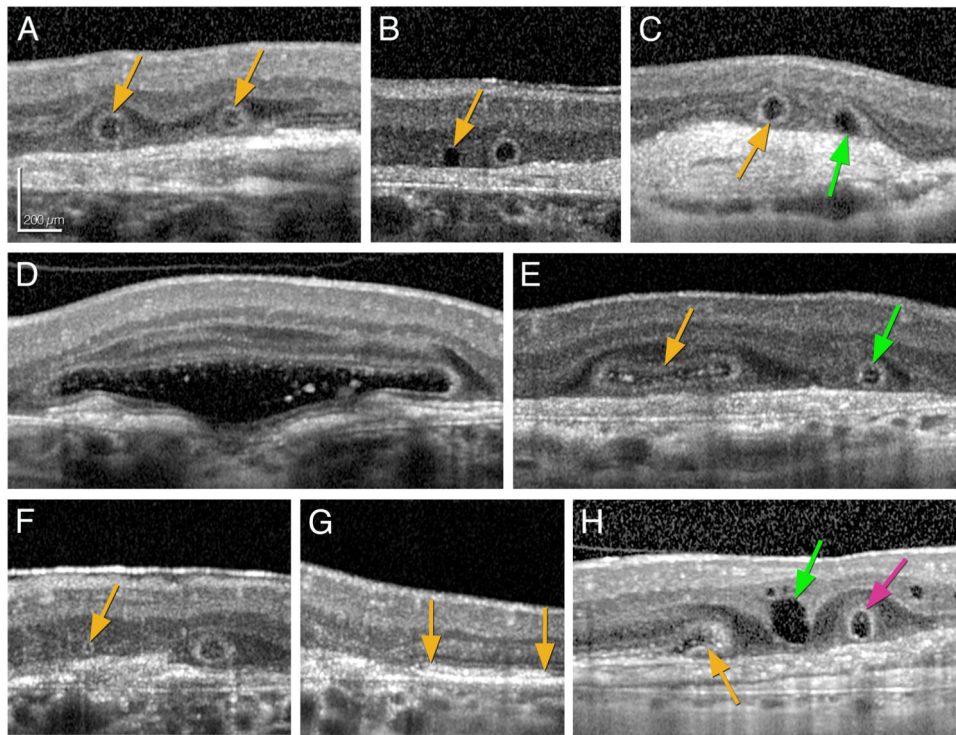


**Figure 4. ORT shapes and differentials vs other outer retinal structures in advanced AMD**  
 All images were obtained in a Spectralis OCT (with signal averaging). All OCT images are shown in the 1:1 pixel mode for better illustration. **A.** Two circular cross-sections (orange arrows) with internal hypo-reflectivity (lumen) and bounded by a thick hyper-reflective border, located in the outer nuclear layer (ONL) overlying a fibrovascular scar. **B.** Next to a circular ORT with a hyper-reflective border is a circular cross-section with internal hypo-reflectivity lacking a hyper-reflective border (orange arrow), which is either a cyst or an end-stage ORT. **C.** A circular cross-section with 360° of hyper-reflective border is a closed ORT (orange arrow). An ovoid cross-section lacking hyper-reflectivity on its outer aspect (adjacent to the scar) is an open ORT (green arrow). **D.** A large and ovoid cross-section with hyper-reflective material attached to the upper part of the hyper-reflective border and intra-luminal free floating hyper-reflective material (large ORT). **E-F.** ORT show different forms. **E.** A flat and ovoid cross-section with a hyper-reflective border (orange arrow) has internal hyper-reflective material in the lumen. A circular cross-section has a hyper-reflective border (green arrow). **F.** A cross section of a very small (42 μm in horizontal diameter) ORT with a hyper-reflective border (yellow arrow). **G.** A cross-section showing a preserved hyper-reflective band (ellipsoid zone, two orange arrows), where the correct orientation of the photoreceptors and their interdigitation with the RPE is still present (photoreceptor island). **H.** A cross-section showing a forming tubulation (forme fruste ORT) with a free edge to scroll (orange arrow) next to an ovoid cross-section with internal hypo-reflectivity lacking a hyper-reflective border, located in the outer plexiform layer (cyst, green arrow). Circular cross-section with a thick hyper-reflective border (pink arrow) in the outer nuclear layer (ORT).

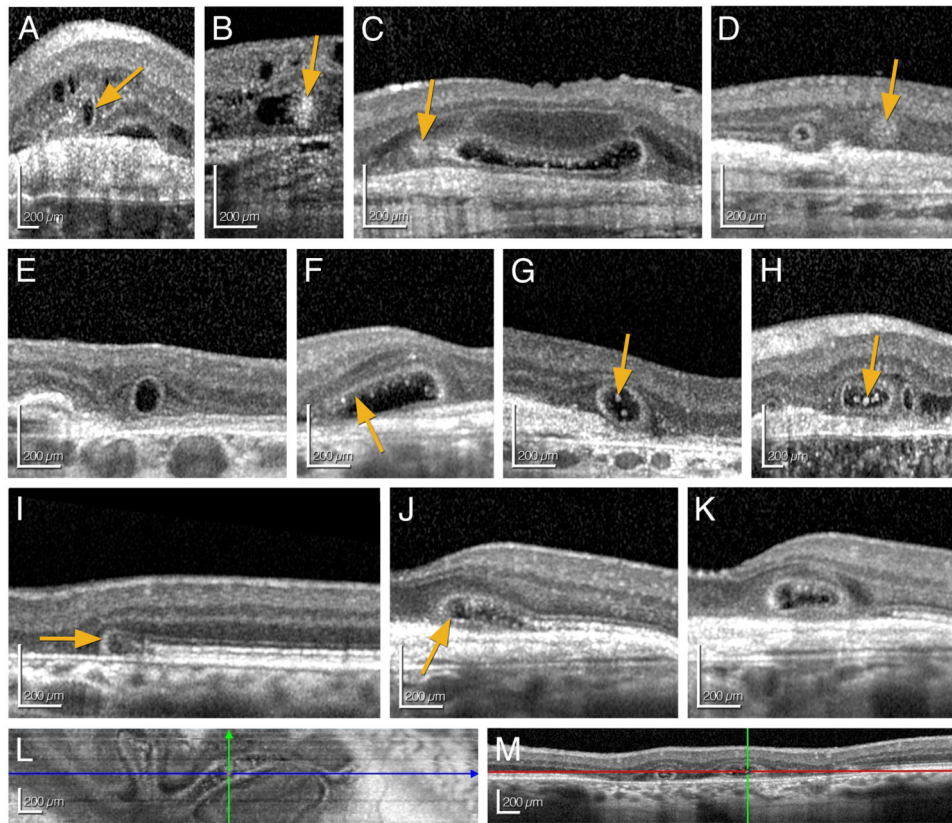


**Figure 5.**

ORT internal contents, associated structures, and formation. **A.** A cross section with a partial hyper-reflective line (orange arrow; asymmetric ORT). **B – D.** Cross-sections of well-defined round homogeneously hyper-reflective clouds (orange arrow) at a variable distance from ORT. **E.** A Cross-section with internal hypo-reflectivity bordered by a hyper-reflective border, (no luminal content). **F.** A cross-section showing hyper-reflective material attached to the hyper-reflective border at the upper part of the ORT (orange arrow). **G – H.** Cross-sections showing intra-luminal free floating hyper-reflective material of different sizes and shapes (orange arrows). **I – K.** Cross sections showing different stages in ORT formation (**J** and **K** are scans 77 μm apart in the same patient). **I.** External limiting membrane (ELM) circles and thickens (free edge scrolling, orange arrow). **J.** More advanced stage in ORT-formation with further scrolling of the free edge (orange arrow), and visibly separating the lumen from the underlying scar by 'embedding' the ORT in the ONL. **K.** Circular cross-section of an ORT with a visible 360° hyper-reflective band (closed and completely formed ORT). **L.** En face OCT showing ORT branch. Blue line indicates B-scan shown in **M.** **M.** Scan through the ORT branch shown in **L** (Two lumen are shown).

**Table 1**  
**ORT correspondences in histology and OCT**

ORT feature	Histology figure	OCT figure
Closed	1B, 1C, 1D, 1E, 1F, 1G, 1H, 2B, 2D, 3A	4A, 4B, 4C, 4D, 4E, 4F, 4H, 5C, 5D, 5E, 5G, 5H, 5K, 5M
Open	3B, 3G, 3D,	4C, 5F
Asymmetric	3C	5A, 5B
End-stage	1E, 1F, 1G	Possibly 4B (right); needs scans from earlier in time for certainty
Island	3F	4G
Cyst	3A	4H, 5A, 5B
Flat or ovoid shape	3E	4D, 4E, 5C
Nearby spheroid cones Reflectivity clouds	1C	5B, 5C, 5D
Scrolled hyper-reflective bands		4H, 5I, 5J
Small cross-section	1E, 1F	4F
Branch	3D	5L, M
Luminal cells hyper-reflective contents	1B, 1G, 1H, 2B	4A, 4D, 4E, 4H, 5G, 5H
Nascent	1B, 3E (left)	
Mature	1D, 1H, 3B, 3C, 3F, 3G (right)	
Degenerate	1C, 1E, 1G, 2B, 3A, 3D, 3E (right), 3G (left)	
End-Stage	1F	